***Journal of Iberian Geology* 42 (2) 2016:** 171-186
http://dx.doi.org/10.5209/rev_JIGE.2016.v42.n2.51642

www.ucm.es/info/estratig/journal.htm
ISSN (print): 1698-6180. ISSN (online): 1886-7995

Journal of Iberian Geology
AN INTERNATIONAL PUBLICATION OF EARTH SCIENCES

Strontium isotopes and sedimentology of a marine Triassic succession (upper Ladinian) of the westernmost Tethys, Spain

Y. Sánchez-Moya[1,2]*, M.J. Herrero[3], A. Sopeña[2]

[1]*Departamento de Estratigrafía. Facultad de Ciencias Geológicas. Universidad Complutense. 28040 Madrid (Spain).*
[2]*Instituto de Geociencias, CSIC-UCM. José Antonio Nováis, 12. 28040 Madrid (Spain) .*
[3]*Departamento de Petrología y Geoquímica. UCM. Facultad de Ciencias Geológicas. Universidad Complutense. 28040 Madrid (Spain.*

*e-mail addresses: yol@ucm.es (Y.S.-M., *Corresponding author); mjherrer@ucm.es (M.J.H.); sopena@ucm.es (A.S.)*

Received: 11 January 2016 / Accepted: 28 July 2016 / Available online: 10 August 2016

Abstract

Chemical Stratigraphy, or the study of the variation of chemical elements within sedimentary sequences, has gradually become an experienced tool in the research and correlation of global geologic events. In this paper $^{87}Sr/^{86}Sr$ ratios of the Triassic marine carbonates (Muschelkalk facies) of southeast Iberian Ranges, Iberian Peninsula, are presented and the representative Sr-isotopic curve constructed for the upper Ladinian interval. The studied stratigraphic succession is 102 meters thick, continuous, and well preserved. Previous paleontological data from macro and micro, ammonites, bivalves, foraminifera, conodonts and palynological assemblages, suggest a Fassanian-Longobardian age (Late Ladinian). Although diagenetic minerals are present in small amounts, the elemental data content of bulk carbonate samples, especially Sr contents, show a major variation that probably reflects palaeoenvironmental changes. The $^{87}Sr/^{86}Sr$ ratios curve shows a rise from 0.707649 near the base of the section to 0.707741 and then declines rapidly to 0.707624, with a final values rise up to 0.70787 in the upper part. The data up to meter 80 in the studied succession is broadly concurrent with $^{87}Sr/^{86}Sr$ ratios of sequences of similar age and complements these data. Moreover, the sequence stratigraphic framework and its key surfaces, which are difficult to be recognised just based in the facies analysis, are characterised by combining variations of the Ca, Mg, Mn, Sr and $CaCO_3$ contents

Keywords: Strontium isotope, Chemostratigraphy, Muschelkalk, Middle Triassic, Iberian Ranges

Resumen

La Quimioestratigrafía o el estudio de la distribución geoquímica de los elementos y sus variaciones en las secuencias sedimentarias, se ha convertido en una herramienta de interés para la investigación y correlación de eventos geológicos globales. En este trabajo, se analizan los valores de la relación isotópica $^{87}Sr/^{86}Sr$ de los carbonatos marinos en facies Muschelkalk del Triásico del sureste de la Cordillera Ibérica que han sido atribuidos al Ladiniense superior. La sucesión tiene un espesor de 102 m, es continua y está muy bien preservada. Los datos paleontológicos de estudios previos basados en macrofauna de ammonites y bivalvos, y en microfauna de foraminíferos, conodontos y asociaciones palinológicas, sugieren un intervalo de tiempo Fassaniensen-Longobardiense. El análisis detallado de la petrología y geoquímica de los carbonatos, demuestra que la mayor parte de la sucesión no ha sufrido una diagénesis intensa. La variación vertical de las relaciones isotópicas del contendido en Sr indica un cambio paleoambiental significativo en las características químicas del mar triásico del Tetis para este sector. La relación $^{87}Sr/^{86}Sr$ es de 0.707649 en la base de la sección, aumenta ligeramente en sentido vertical hasta valores de 0,707741 para disminuir rápidamente a 0,707624. En el techo de la serie las cantidades aumentan de nuevo hasta 0,70787. Los valores obtenidos de la relación $^{87}Sr/^{86}Sr$ en los primeros 80 metros de la sucesión, coinciden con las relaciones obtenidas en secuencias de la misma edad en otros ámbitos del mar del Tetis. La combinación de las variaciones de elementos traza de Ca, Mg, Mn y Sr y del contenido total $CaCO_3$ ha permitido además, caracterizar geoquímica y mineralógicamente el análisis secuencial y el reconocimiento de las superficies que limitan las secuencias deposicionales para la región estudiada.

Palabras clave: Isótopos de estroncio, Quimioestratigrafia, Muschelkalk, Triásico medio, Cordillera Ibérica

1. Introduction

Chemical stratigraphy, the study of elemental composition and isotopic ratios within sedimentary sequences, has become a useful tool in the research and correlation of global geological events, although higher resolution datasets are needed to construct the best curves of the evolution of isotope ratios and elements of particular interest to correlations. This article includes a study of $^{87}Sr/^{86}Sr$ ratios, trace elements and mineralogies of bulk carbonate samples. Despite the fact that the $^{87}Sr/^{86}Sr$ trend has potential for dating and correlating rocks, only one study has used strontium isotopes in northern Spain (Sopeña *et al.,* 2009) trying to date a Triassic succession. The strong diagenetic transformations, essentially dolomitization, that affect most of the marine carbonates comprising the Triassic sequences of the Iberian Peninsula are the main reason for the lack of studies dating the succession based on $^{87}Sr/^{86}Sr$ ratios. Nevertheless, there are some outcrops where the composition of most of the stratigraphic succession consists of limestones and dolostones where it is possible to develop a Sr-isotope stratigraphy with adequate assurance that the original isotopic signal has been preserved. This study presents data from the Muschelkalk in the SE of Spain, in the Alpera-Montealegre del Castillo region (Fig. 1), where the marine carbonates are considered to preserve their original geochemical signal and the $^{87}Sr/^{86}Sr$ ratio permits dating, establish correlations, determine facies relationships and make palaeoenvironmental reconstructions.

Seawater chemistry has varied with global climate throughout Earth's history, with ion ratios such as Mg/Ca and Sr/Ca useful for determining paleo-ocean conditions (Cohen *et al.,* 2002). Their variations in seawater are related to carbonate sedimentation and represent the main factor involved in the regulation of the mineralogical nature of inorganic $CaCO_3$ (MacKenzie and Pigott, 1981; Wilkinson and Given, 1986), and they are as well of great influence to the marine biota and the distribution of carbonate sediments (Lowenstein *et al.,* 2001). Variations in the Mn supply during sedimentation has been used as an indication of continental or hydrothermal origin of the materials, as well as being indicative of oxygen contents, where reducing environments lead to formation of Mn-poor carbonates, whereas oxidizing environments lead to formation of Mn-rich sediments (Renard, 1985). In a similar way, strontium isotopic composition of ancient seawater has served as a proxy for understanding the tectonic evolution of the Earth system as well as a tool for stratigraphic correlation (Korte *et al.,* 2003). The $^{87}Sr/^{86}Sr$ signature of seawater reflects fluctuations in the relative importance of strontium fluxes and their isotope ratios into the ocean (Burke *et al.,* 1982; Veizer *et al.,* 1999). These are 1) the riverine input of radiogenic Sr due to continental silicate weathering and 2) the "mantle Sr" from hydrothermal circulation at mid-ocean ridges (Faure, 1986), likely coincident with the second-order sea level fluctuations (Gaffin, 1987). There are as well Sr fluxes from groundwater and from carbonate diagenesis (Veizer, 1989). Uplift phases are coincident with falling sea levels, exposing large areas and the subsequent erosion a genesis of detrital material.

This study focuses on the analysis of a Triassic succession located in the southern part of the Iberian Range. From the Middle Permian to Early Triassic, the Iberian Plate was near the western margin of the Tethys Sea, which was located close to the intertropical convergence zone (Stampfli and Borel, 2002). A complex system of rift basins developed in Central and Western Europe, produced by the extensional collapse of the Variscan Belt and the westward advance of the Neotethys

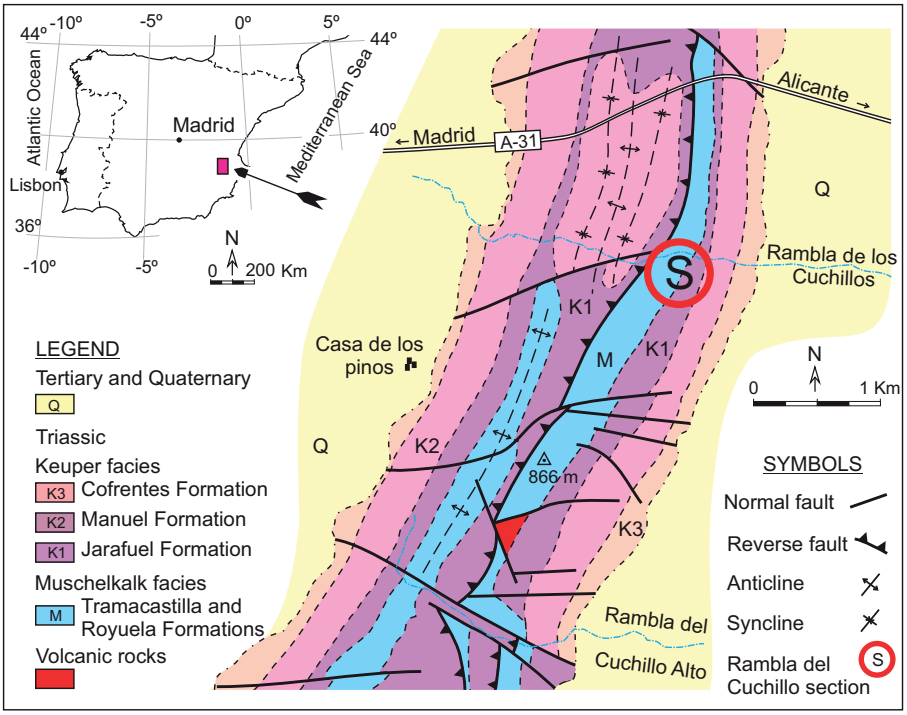

Fig. 1.- Geologic setting and location of the "Rambla del Cuchillo" section. The outcrop corresponds to the Triassic of Alpera-Montealegre del Castillo region. Section coordinates: 38º 52' 07.38" N/1º 15' 14.86" W

(Ziegler and Stampfli, 2001). In the Iberian Plate, three main rift systems accommodated a complicated Permian to Cenozoic record that, after tectonic inversion, formed the Betics, Pyrenean–Cantabrian mountain belt, the Catalan Coastal Ranges and the Iberian Ranges (De Vicente *et al.,* 2009). Triassic deposits in the Iberian Peninsula have been extensively studied from a sedimentological point of view (Ramos *et al.,* 1986; López-Gómez *et al.,* 2002; Sopeña, 2004), and their lithostratigraphic divisions are characterized and used as references for Triassic sequences from south Germany and adjacent areas in Europe (Ziegler, 1990; Aigner and Bachmann, 1992; López-Gómez *et al.,* 2002; Sopeña, 2004), being the classic Germanic-type terms used as facies descriptions and not as time intervals. During the Early Triassic, the Iberian Microplate was covered by sandstones and conglomerates of Buntsandstein character. During the Middle Triassic two marine transgressions advanced from the east and covered the eastern part of the Iberian Peninsula during which Muschelkalk carbonates were laid down (Sopeña *et al.,* 1988; López-Gómez *et al.,* 2002; Bourquin *et al.,* 2011; Mercedes-Martín *et al.,* 2014). Subsequently, during the overall regression that took place in the Upper Triassic, red and grey clays and marls with anhydrite, gypsum and sometimes sandstones were deposited. This upper unit is the Keuper, which, just like the Muschelkalk and Buntsandstein, contains materials analogous to those deposited in a large part of Western Europe during the same time span (Bourquin *et al.,* 2011; Escavy *et al.*, 2012; Arche and López-Gómez, 2014). The ages of the different Triassic units are based on biostratigraphy (López-Gómez *et al.,* 2002). Triassic deposition culminated with an upper carbonate sequence of Norian age, Zamoranos Formation, defined by Pérez-López *et al.* (1992) in the study area and revised by Pérez-López *et al.* (2012).

The Alpera-Montealegre del Castillo area is located in the southern part of the Iberian Range, in the northeastern Prebético Zone (Fernández and Pérez-López, 2004). The Triassic stratigraphic succession in this area is composed of three main lithofacies: the lower part of the succession corresponds to the Buntsandstein facies, the middle part to the Muschelkalk, and the Keuper facies form the upper part of the succession. According to Sopeña *et al.* (1990), in the study area (Fig. 1) the Muschelkalk consists of a lower dolomitic unit called Tramacastilla Fm. and an upper unit, Royuela Fm., composed of limestones, dolostones and marls. Both units constitute the Siles Formation defined by Perez-Valera (2005) and include the "Rambla del Cuchillo" section (Coordinates: 38º 52' 07.38" N/1º 15' 14.86" W, Elevation: 795 m NM, Fig. 2), which has been analyzed from a sedimentological, petrographical and geochemical points of view.

The aim of this work is to present a new section of reference of the Sr-isotope stratigraphy of the mid-Triassic carbonate platforms of the western Tethys in an area from which very little Sr data exist due to the commonly strong dolomitization processes that have undergone the carbonates forming the sequences.

2. Materials and methods

The characteristics of the outcrop permit a very detailed study of the main vertical facies successions and determine the environments of deposition. For the geochemical characterisation of samples, calcite mudstones and wackestones have been chosen as they are considered to retain more accurately their original isotopic composition due to their lower permeability character in comparison to associated grain-supported rocks (Fig. 3). Previous to any isotopic analyses, the amount of diagenetic phases in each sample was assessed by a combination of petrographical observations, SEM, cathodoluminescence, ICP and XRD analyses. Conventional petrography analyses were performed on 20 thin sections stained with alizarin red to differentiate calcite from other carbonate minerals, and they were as well observed under fluorescence and cathodoluminescence. Scanning electron microscopy (SEM) observations were made on gold-coated samples using a JEOL 6400 electron microscope working at 20 kV and with a resolution of 35 Å. ICP analyses, performed at the CAI of Técnicas Geológicas UCM, was used to obtain the trace elements contents, and data was submitted in ppm. The samples were analysed by the BRUKER Aurora Elite Mass spectrometer. Powdered samples were mineralogically characterized using a Philips PW-1710 X-ray diffraction (XRD) system operating at 40 kV and 30 mA, and employing monochromated CuKα radiation. XRD spectra were obtained from 2º to 66° 2θ. The mineral phases were identified by comparing the experimental reflections spacing with those from the Index X-Ray data for minerals (JCPD). Several limestone samples from the carbonate units were analysed by the Geochronology and Isotopic Geochemistry Laboratory of the Complutense University (Madrid, Spain). Samples dissolution was carried out in hydrochloric acid (2.5N) on a hotplate at 80 °C to complete dryness. Then, the residue was dissolved in 2ml of 2.5N HCl and centrifuged (10 minutes at 4000 rpm) to eliminate possible undissolved remains. Finally, the Sr separation of the supernatant was performed through a chromatography column using DOWEX AG-50Wx12 (200/400 mesh) resin (previously calibrated) along with 2.5N HCl as eluent. The resultant concentrated Sr was dried and dissolved in 1 µl of 1M phosphoric acid and the isotopic ratios were obtained by mass spectrometry Thermal ionization-VG TIMS SECTOR 54, with 5 Faraday detectors through the measuring system by dynamic multicollection (McArthur *et al.,* 1998). The values of Sr were corrected for possible isobaric interference from ^{87}Rb and normalized to the value $^{86}Sr/^{88}Sr = 0.1194$. During analysis, the isotopic standard NBS-987 was measured and a value of 0.710285 ± 0.00004 was obtained at level 2σ for the $^{87}Sr/^{86}Sr$ ratio for a number of data of n=7. This coincides with the value obtained for the same standard in the laboratory (0.710254 ± 0.00004). The analytical error for the $^{87}Sr/^{86}Sr$ ratio was 0.01 %. Statistical regression was performed using LOWESS (Locally Weighted Scatterplot Smoother) V3 software (Cleveland, 1979; Chambers *et*

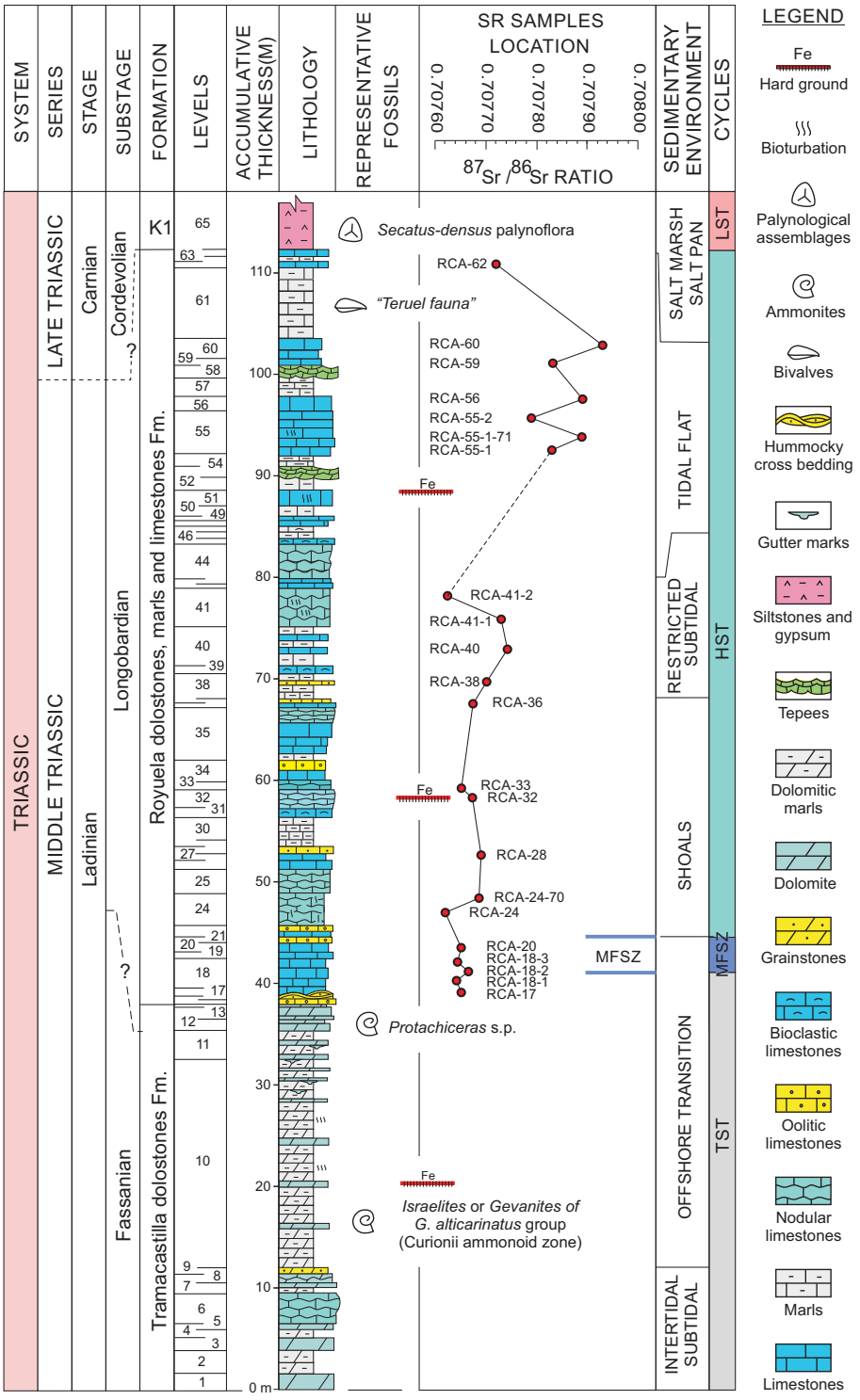

Fig. 2.- Stratigraphic section of "Rambla de Cuchillo" and the $^{87}Sr/^{86}Sr$ curve. The samples, numbered according to corresponding level, are the ones used for the geochemical and mineralogical diagrams. TST: Transgressive Systems Tract. MFZ: Maximum Flooding Zone. HST: Highstand Systems Tract. LST: Lowstand Systems Tract.

al., 1983; Thisted, 1988; Cleveland *et al.,* 1992), to obtain numerical ages with 95 % confidence limits for any given $^{87}Sr/^{86}Sr$ value (McArthur *et al.,* 2001).

2.1. Preservation of carbonate original composition

In order to establish the geochemical and the carbonates isotopic signals as a direct correlation of the sea water from the time at which they formed (which is one of the aims of this work) it has to be demonstrated that the carbonates preserve their original geochemical composition and even the existence of subtle diagenetic alteration that may have overprinted the primary palaeoceanic geochemical signal (Veizer, 1995; Bruckschen *et al.,* 1999). The degree of diagenetic alterations is mainly controlled by the water-rock ratio (Banner and Hanson, 1990), that is, the "open-ness" of the diagenetic system, and it can vary between different constituents of a carbonate (Veizer, 1983).

The first attempt searching for diagenetic overprints was the establishment of the samples Preservation index (PI of

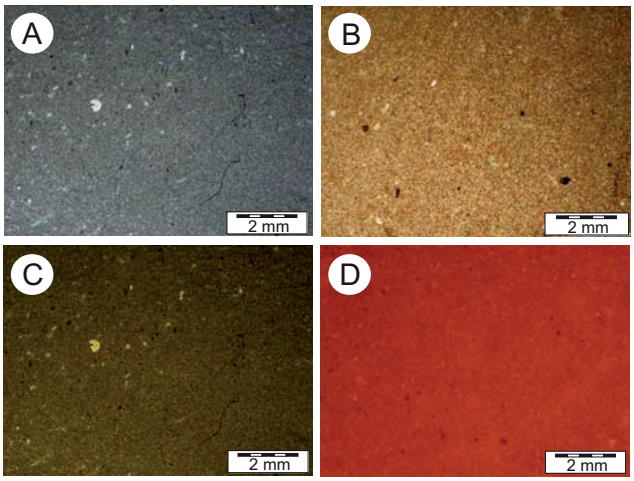

Fig. 3.- Photomicrograph from a section of one the studied mudstones. A, Planar polarized light. The sample is mostly composed of micrite and no major diagenetic processes are detected. B, Thin section under cross polarized light where the calcitic character of the sample is observed. C, Same thin section as B, under fluorescence light. There are no organic materials of interest. D, Sample under cathodoluminescence showing the dull character of the components, indicating that the sample did not undergo diagenetic modifications.

Cochran *et al.,* 2003) based on petrological and SEM characterisation. As PI changes from 5 to 1 (excellent to bad preservation), the $^{87}Sr/^{86}Sr$ ratio decreases, together with a lowering of the Sr/Ca ratio (Cochran *et al.,* 2010). In this study, most samples have PI higher than 3 with no major alterations, and normally samples with PI higher than 3 do not show significant variations of the $^{87}Sr/^{86}Sr$ ratio (Cochran *et al.,* 2010). Although the Sr/Ca seems to show certain inverse correlation with a decrease of the $^{87}Sr/^{86}Sr$ ratio (Fig. 4A), when analysing the Sr/Ca values in detail it is noted a sharp fall. Looking at the correlation of Sr/Ca ratio with the $^{87}Sr/^{86}Sr$ there are two differentiated populations (Fig. 4A1 and 4A-2): it is appreciated there is no correlation of the basal part of the data (up to samples from meter 80 in the section), indicating no significant diagenesis of this samples; meanwhile, the data towards the top seem to have some inverse correlation that could be indicating a diagenetic overprint of these samples. Trace element contents have as well been analysed in detail to determine possible postdepositional overprints. The samples from the lower part of the section (up to meter 80) in general show Sr contents with average values of 500 µg/g, and Mn contents with average values of 30 µg/g (Table 1). Corresponding Mn/Sr ratios are also < 2 µg/g (average value of 0.06). These elemental values of the lower part of the section are higher than the minimum Sr content (> 150 µg/g) and far below the maximum Mn content (250 µg/g) commonly used as cut-off limits (Korte *et al.,* 2003; Brand and Veizer, 1980) indicating diagenetic alterations. The Mn/Sr values appear as well much lower than the maximum ratio (2) of the cut-off limit suggested by Jacobsen and Kaufman (1999) indicative of diagenetic modifications.

As a final test to discriminate any postdepositional transformation of the carbonates element ratios (Mg/Ca and Mn/Ca) were also plotted vs. $^{87}Sr/^{86}Sr$ (Fig. 4). The lack of correlation of element ratios contents with the $^{87}Sr/^{86}Sr$ curve

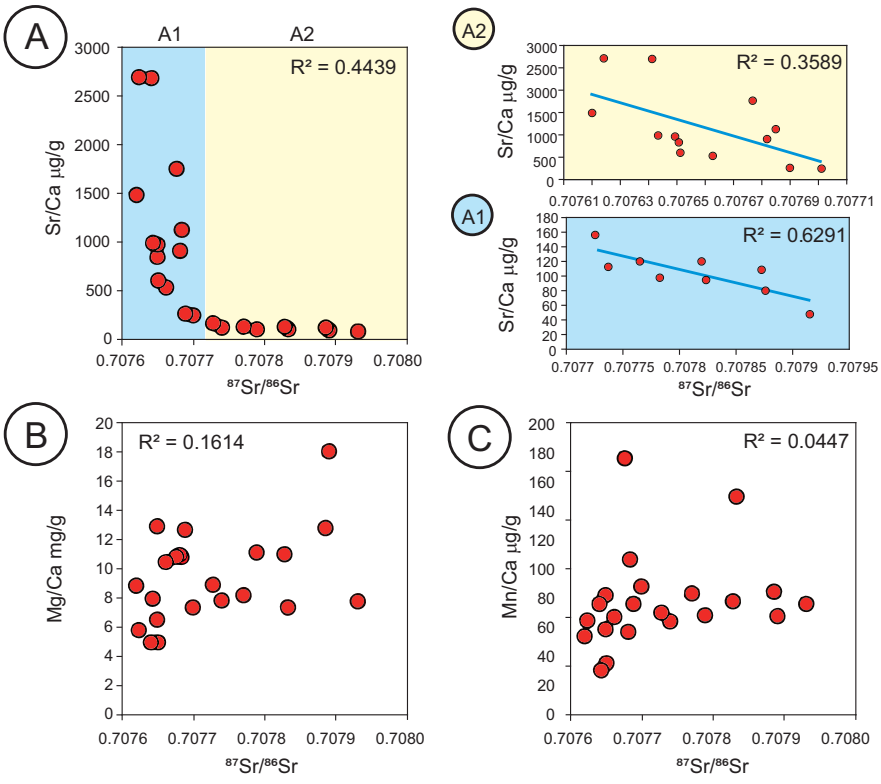

Fig. 4.- Crossplots of 87Sr/86Sr versus the different elements ratios. A, Sr/Ca ratio. A1, Sr/Ca ratio for values of the section up to meter 80. A2, Sr/Ca ratio from meter 80 to the top. C, Mg/Ca ratio. D, Mn/Ca ratio.

Sample	Height	%$CaC0_3$	$^{87}Sr/^{86}Sr$	%Ca	Ca(µg/g)	Si(µg/g)	Mg (µg/g)	Fe(µg/g)	Mn(µg/g)	Sr(µg/g)
RC-62	112.27	90	0.707772	39.15	391500	4700	3100	1500	30	18
RC-60	103.93	87	0.707933	38.27	382700	18900	7000	4000	26	31
RC-59	102.82	92	0.70783	37.79	377900	12600	4900	3000	32	40
RC-56	98.93	90	0.707893	38.59	385900	8700	2900	2500	58	36
RC-55-2	97.27	90	0.70779	38.37	383700	10400	4300	2300	30	47
RC-551-71	95.60	-	0.707887	38.03	380300	12700	4300	2500	26	36
RC-55-1	93.93	89	0.707834	38.39	383900	11400	3200	1800	32	45
RC41-2	80.04	92	0.707624	38.73	387300	8400	3100	2100	25	43
RC-41-1	77.27	90	0.707729	38.5	385000	10700	3500	1900	27	59
RC-40	74.49	91	0.707741	38.58	385800	9600	2900	2700	34	91
RC-38	71.71	89	0.7077	38.04	380400	12300	4900	2900	29	98
RC-36	68.93	89	0.707676	38.21	382100	12100	4200	2500	41	426
RC-33	61.16	90	0.70765	38.6	386000	8000	4300	2000	22	347
RC-32	59.49	88	0.707681	37.3	373000	17800	4100	3200	66	652
RC-28	54.21	88	0.707689	38.53	385300	8500	4100	2400	26	201
RC-24-70	50.16	-	0.707684	39.15	391500	5200	2000	1400	14	234
RC-24	48.66	91	0.70762	38.87	388700	6400	2600	1700	23	327
RC-20	45.04	91	0.707651	38.94	389400	4600	5100	2900	32	375
RC-18-3	43.66	91	0.707643	39.3	393000	4600	3200	1100	12	385
RC-18-2	42.82	91	0.707662	39.11	391100	5400	2000	900	30	1049
RC-18-1	41.99	89	0.707641	38.51	385100	7200	2300	1700	25	1038
RC-17T	40.60	90	0.707649	38.71	387100	6800	3500	3300	21	572

Table 1. Geochemical data of samples from the Rambla del Cuchillo section

suggests as well none or minimal postdepositional alteration (Rosales *et al.,* 2001; Nieto *et al.,* 2008). The effect of eo or telodiagenetic processes by meteoric water in the different carbonate components commonly is reflected by increasing textural alteration of the matrix that change successively from micrite to microsparite, to minor pseudosparite and/or to precipitation of interparticle sparite cement. This physical evolution is accompanied by concomitant changes in trace element composition, in particular, Sr decreases and Mn increases. These elements trend change is observed in the upper part of the section (from meter 80 towards the top of the succession), and therefore, and as indicated herein, it is inferred diagenetic overprint of this upper part of the section.

3. Results

3.1. Stratigraphic and sedimentological setting

Despite differences between areas and units, Middle Triassic carbonate systems in Spain, Muschelkalk facies, have been interpreted by all authors as representing a carbonate epeiric platform with a ramp profile (Sopeña *et al.,* 1988; Calvet *et al.,* 1990; López-Gómez *et al.,* 2002; Pérez-Valera and Pérez-López, 2008, Pérez-López and Pérez-Valera, 2012; Pérez-López *et al.,* 2012; Escudero-Mozo *et al.,* 2015). Within this context, the Alpera-Montealegre del Castillo Muschelkalk carbonates were formed in a gentle slope epicontinental carbonate platform. The main lithofacies and depositional subenvironments (Fig. 2), from base to top, are briefly summarized as follows:

Intertidal to subtidal deposits (levels 1 to 9)

The lower Muschelkalk deposits overlie Buntsandstein mudstones and sandstones, and consist of nodular bedded dolostones and green to grey marls. Dolostones show undulating and flatter algal lamination, bird eye structures, ripple lamination and bioturbation. A fossiliferous level, yielding mainly fragments of bivalves and gastropods, is located at the top. These deposits were formed as microbial mats in a subtidal to intertidal environment of a shallow platform system, associated to planar-laminated stromatolites (Calvet *et al.,* 1990). These sediments correspond to very shallow upper shoreface to foreshore carbonate environments.

Offshore transition (levels 10 to 20)

This part of the succession is characterized by offshoal and foreshoal deposits and corresponds to a classical shoreface to offshore transition. At the base, the low energy sequence (Fig. 5, sequence-type e) is composed of interbedded green marls, thin grey dolostones and marly-dolostones. At the lower levels, the facies display parallel and ripple lamination. Bioturbation and poorly preserved small fauna remnants are present, and some intervals have brachiopods accumulation and iron-oxide mineralization. All these sedimentary

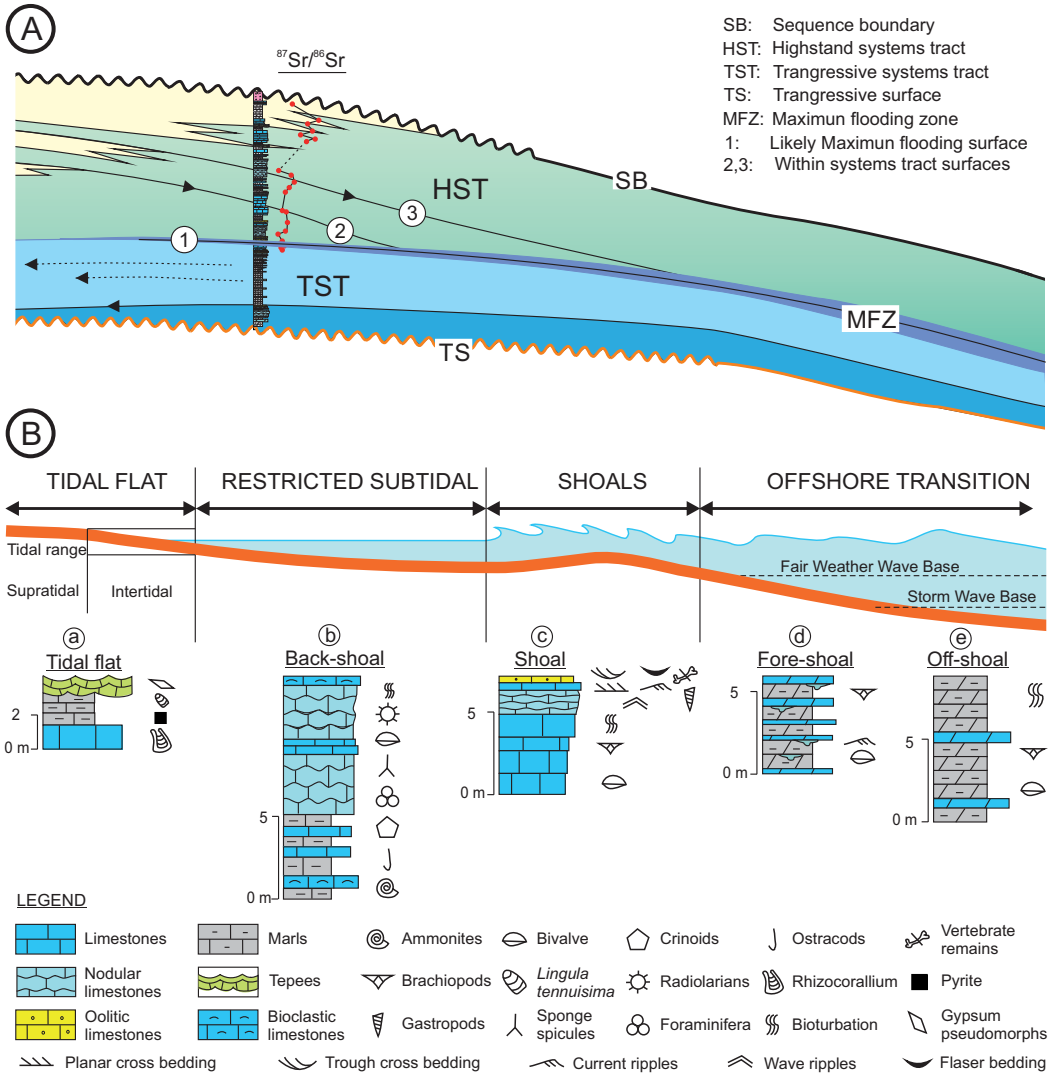

Fig. 5.- Depositional sequence model for Muschelkalk epeiric carbonate platform at "Rambla del Cuchillo" section. A, Idealized depositional model. B, Depositional sub-environments sketch and main facies associations.

materials were deposited under low energy conditions but occasionally distal storm deposits (show parallel and ripples lamination) were formed in this area. The dark colour indicates oxygen-depleted or anaerobic condition. Within these facies, at 15 meters from the base of the succession, appears *Gevanites* (Curionii Zone, Brack *et al.,* 2003; Brack *et al.,* 2005), which serves to date biostratigraphically this level. Based on these characteristics and the relationship with surrounding facies, these deposits are interpreted as low energy associations formed bellow storm wave-base offshore deposits. In the palaeoenvironmental reconstruction of the Alpera-Montealegre del Castillo Upper Ladinian carbonate platform, these facies are interpreted as offshoal deposits.

Overlaying the previous sequences appear different moderate to high-energy facies, interpreted as storm deposits interbedded with low energy facies. The storm facies appear as three distinct facies associations. The first storm facies, the most prevalent and located on top of offshore deposits (at a height of 30 m), is composed of gutter and pot casts facies, with small isolated erosional structures that are filled by fine grained dolostones with bivalves and brachiopod fragments and/or limestones with shell debris (Fig. 5 sequence-type d). The second type of storm facies is characterised by bioclastic limestones with hummocky structures. The limestones are packstones to wackestones interbedded with marls, with abundant bivalves, gastropods, brachiopods, echinoderms, sponge spicules, crinoids, ostracods and foraminifera. Profuse bioturbation is present too. Hummocky cross-stratification, typical feature of storm deposits formed just above the storm wave base level, is present at some levels (e.g. level 17). The third type of storm facies is composed of thin limestones with shell-debris. It appears at top of storm facies 1 and 2, or even cross cutting them.

These materials are interpreted as storm deposits formed in shallow waters, probably formed just below fairweather wave-base, between the shoreface and offshore transitional zones correlated to similar storm dominant successions in the Prebetic areas (Pérez-López, 2001; Pérez-Valera and Pérez-

López, 2008; Pérez-López and Pérez-Valera, 2012). According to Myrow (1992a), gutter and pot facies are generated by rotary and helical flows during storms. Storm facies 1 and 2 represent a progressive step towards an area of storm dominated conditions with higher energy water levels (Aigner and Futterer, 1978; Myrow, 1992 a, b; Pérez-López, 2001). Storm facies 3 is interpreted as deposits where bioclasts were concentrated by being winnowed by storm waves. Storm deposits are placed mainly at the fore-shoal sub-environment.

Shoals (levels 21 to 36)

The overlying facies association is characterised by moderate to high energy deposits represented by oolitic limestones and locally appear facies composed of bioclastic packstones and grainstones. Both facies associations have planar and trough cross-bedding stratification, including low-angle and current and wave ripples as well as flasher structures. Bioclastic fragments, bivalves, gastropods, brachiopods, echinoderms, ostracods, nodosarids and pellets, among other fossil remnants, are abundant (Fig. 5, sequence-type c). No emersion marks were found, but in the two last sequences stromatolite lamination can be observed at tops, pointing to shallow (subtidal to intertidal) conditions, as currently occur in Bahamas. Vertebrate bones appear in the last sequence. The facies indicate sedimentation and reworking due to frequent high-energy hydrodynamic condition periods. These deposits are interpreted as oolitic-bioclastic shoal patches formed in the shoal zone, which suggests the formation of a thin, high energy shore-parallel shoal complex and the genesis of an open sheltered environment located behind it, though there was not a major barrier. Interbedded bioturbated mudstones indicate calm periods.

Restricted subtidal (levels 37 to 43)

This facies association is composed of black-muddy limestones, packstones to wackestones, and marls that appear locally bioturbated. They display lamination at their bases and change upward to nodular bedding (Fig. 5, sequence-type b). These are interpreted as being deposited in a sheltered environment or backshoal area under open marine conditions, meaning the shadow back part of a shoal complex towards the continent. The nodular texture is the result of intense bioturbation and/or diagenetic overprints, although this last possibility is less compatible with the petrographic observations. Parallel lamination and current and wave ripples are also frequent. The interbedding of grainstones and muddy sediments indicates the existence of spill-over lobes produced during storm conditions. The low-energy backshoal deposits also contain limestone layers with thin shell-debris of valves that appear horizontal and concave-down, which correspond to storm deposits where bioclasts were concentrated after being winnowed by storm waves. The low-energy backshoal facies are interpreted to represent fair-weather deposits.

Tidal Flat (levels 44 to 64)

Towards the uppermost part of the "Rambla del Cuchillo" Muschelkalk section, the backshoal facies association changes to a succession of grey to green marls that are capped by a muddy limestone. Pyrite, halite p*seudomorphs*, shell-debris, current ripples, wave and flasher structures and *Rhizocorallium irregulare,* are the most prominent features characterizing the muddy limestone. This facies formed in the intertidal to supratidal part of a platform (Fig. 5, sequence-type a). *Rhizocorallium* rich beds, typical of quiet environments such as restricted subtidal areas, appear characteristically interbedded with deposits formed under intense storm activity (Rodríguez-Tovar and Pérez-Valera, 2008). Sparse pyrite crystals indicate oxygen-depleted local conditions, although it is more likely that reducing conditions were caused by the presence of large amounts of organic matter in the tidal flats. This facies association displays the progressive transition towards supratidal environment.

The last few meters of the succession show a predominance of intertidal to supratidal facies. These are composed of laminated yellowish dolomitic marls, ochre dolostones and dolomitic marly and mudstone beds. Marls contain thin limonitic layers with accumulations of the brachiopod *Lingula*, which is typical of the upper Muschelkalk facies in the Iberian Range (Márquez-Aliaga *et al.,* 1999). Ochre dolostone beds show mud cracks, tepees and tepee breccias. Lithology and sedimentary structures indicate an intertidal environment, being the mud cracks, tepees and tepee breccias related to supratidal aerial exposure conditions (Pratt and James, 1986). A transition from burrowed low energy deposits to supratidal dolomicrites indicates a shallowing-upward trend. These deposits represent the coastal systems progradation over a gentle slope platform.

3.2. Biostratigraphic data

The biostratigraphy of the "Rambla del Cuchillo" section is established by the presence of ammonites (Goy, 1995) and palynological associations that have been found in the lower unit of the Keuper, K1, within the clays and gypsum deposits of the Jarafuel Fm. (Pérez-López, 1996). At 15 meters from the base of the section (Fig. 2), appears *Israelites* and *Gevanites* from the group *G. altecarinatus,* attributed by Pérez-Valera *et al.* (2005) to the Curionii zone of Early Ladinian age (Fassaniense). The base of the Curionii zone has been accepted as a GSSP boundary (Global Stratotype Section and Point) by the IUGS (Brack *et al.,* 2003). A few meters upwards, Goy (1995) cites the presence of *Protrachiceras* sp. with other fauna such as bivalves, brachiopods, gastropods, equinoderms, foraminifera, and ostracods. This fauna is not age indicative but is characteristic of Ladinian sequences from other parts of the Iberian Range and the Betic Cordillera (Márquez-Aliaga and Ros, 2003; Márquez-Aliaga *et al.,* 1999). The faunal association that appears at the top of the

section, within the succession that forms the Royuela Fm., comprises the so-called "Fauna de Teruel" which is characteristic of the Upper Ladinian successions through much of the Iberian Cordillera. This fauna is mainly composed of Tethyan (Alpine) species (Márquez-Aliaga and Ros, 2003) and appears restricted to shallow marine environments.

The palynological assemblages found in the overlying unit (K1, Fig. 2) are characterized by the presence of *Camerosporites seccatus*, *Patinasporites densus* and *Valasporites ignacii* as the most characteristic species (Solé de Porta and Ortí, 1982; De Torres, 1990). This type of assemblage corresponds to the so named "secatus-densus" palynoflora by Besems (1981a, b) and is characteristic of the Early Carnian (Cordevolian) in the Iberian Peninsula (Sopeña *et al.,* 1995) and much of Western Europe (Van der Eem, 1983). Therefore, it can be reasonably ruled out that the succession under study, Muschelkalk facies, was formed during the Late Ladinian time span.

3.3. Petrography

In this study 20 carbonate samples of Late Ladinian age, located between meters 40 and 120 of the section of Figure 2, representing tidal flat to offshore transition zone environments, have been characterised petrographically. According to the textural classification of Dunham (1962) the studied limestones are mainly mudstones and wackestones. We have chosen these kinds of materials due to their lower permeability character compared to those of associated grain-supported carbonates. Fine-grained carbonates usually occur in "closed systems", where mineralogical recrystallization and cementation take place from the same, or similar, porewaters in which the sediment was deposited, and it is inferred there would be a partial or total retention of the original elemental and isotopic compositions (Banner and Hanson, 1990; Marshall, 1992; Wenzel *et al.,* 2000). Consequently, mud-supported carbonates are considered more likely to retain better the original seawater Sr-isotope ratio than associated grain-supported rocks. Moreover, fine-grained carbonates provide the most suitable material for such research because the restricted number of $CaCO_3$ producing organism that live in these environments limits potential diagenetic perturbations (Renard, 1985). The studied samples are a single component assemblage (calcite) with only minor quantities of other minerals.

3.4. Mineralogy and Geochemistry

$CaCO_3$ content and relationship with bedding

The deposits represent a complete range from tidal to offshore depositional environment formed in a carbonate platform setting, where limestone and marl deposits alternate regularly. XRD analyses indicate that these samples are highly $CaCO_3$ pure (87 %-92 % $CaCO_3$ content), and no petrological evidences of dolomitization have been observed (Fig. 3). In general, the $CaCO_3$ content (Table 1) shows vertical shifts that indicate five maximums and five minimums. The $CaCO_3$ content of each unit is in accord with the sequential trends delineated in the outcrop. These lithological slight variations could reflect periodic changes of non-carbonate material supply produced during periods of stable carbonate production (Beltran, 2006; Beltran *et al.,* 2007).

Elemental geochemistry

For this study the Ca, Mg, Mn, Fe and Sr contents were measured in 22 mudstones and wackestones (table 1) and their vertical variations, which should indicate changes in the geochemistry of the waters where the carbonates were formed (Fig. 6). The original carbonate phase is assumed to have precipitated in equilibrium with its coeval seawater, in which case it would have incorporated elemental data and stable isotopes signatures from it. The comparison of the facies analysis with the geochemical and element data can serve to characterise the environmental and geological context where the sequence was formed. The Mg/Ca varies between 5 mg/g and a maximum of 18 mg/g. Although Mg content might introduce some uncertainty when interpreting the geochemical signatures of carbonates (Rausch *et al.,* 2013), our samples have very low Mg values (3.7 µg/g), and therefore, we do not expect to find major uncertainties related to its content. Moreover, Mg/Ca ratios show no changes with preservation variations (Cochran *et al.,* 2010). The inflexions of the curve permit to observe the inverse relationship that exist between the Mg/Ca ratio and calcium carbonate content, with the exception of the base of the section where both curves seem to have similar variations up to meter 45.

The Sr/Ca trend allows discriminating between two parts in the succession. The lower part of the succession, up to meter 80, has Sr/Ca ratio with values around 0.001 and 0.003 µg/g, whereas at the top of the sequence the ratio decreases close to 0 µg/g. When combining the vertical trend of the Sr/Ca ratio and the $^{87}Sr/^{86}Sr$ values a sharp change is observed at meter 80 where tendencies vary drastically. Normally, burial diagenesis leads to a decrease of Sr content, yet the values from deeper parts of the section appear to have higher Sr contents than those samples from the upper part. The general negative up section trend in Sr content observed in the section shows that Sr concentrations reflect, at least in the lower part of the studied succession, seawater Sr/Ca ratio fluctuations (Cochran *et al.,* 2010).

Mn content has values of ~ 25 µg/g at the base of the succession. At a height of 59 m, Mn content has a sharp rise up to 66 µg/g. Higher up it decreases again, with variations that range between 22 and 42 µg/g, up to meter 100, where it increases to 60 µg/g again, followed by a return to the normal values of ~ 20 µg/g. Fe content variations correlate with Mn, having only significant differences in the upper

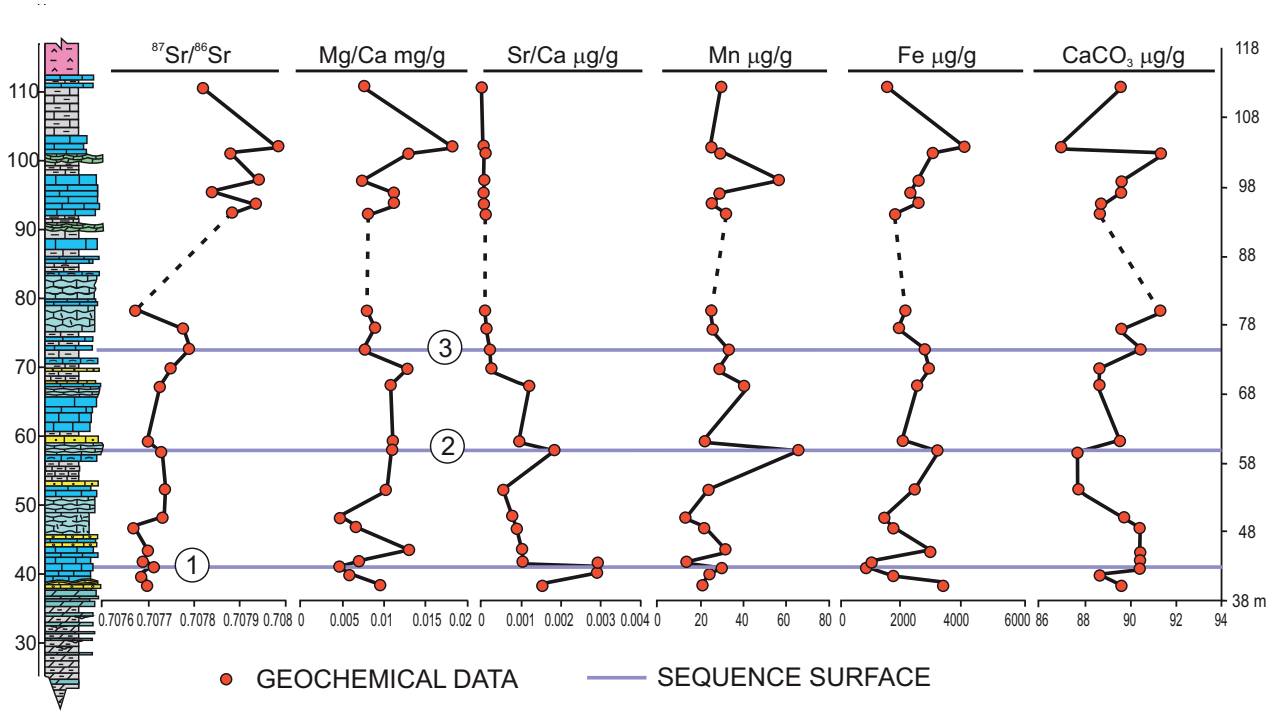

Fig. 6.- Correlation of the "Rambla del Cuchillo" section and the $^{87}Sr/^{86}Sr$ record with curves of various geochemical components (Mg/Ca ratio, Sr/Ca ratio, Mn, Fe and $CaCO_3$ contents).

part of the section, from meter 80. The lower part varies from around 1500 µg/g, with a sharp values rise at meter 58 where it gets up to values between 2000 µg/g and 3300 µg/g. Upwards of that, values are more or less variable but in the same range.

$^{87}Sr/^{86}Sr$ isotopic values

The analysis of the $^{87}Sr/^{86}Sr$ ratio permits the separation of the succession into two main parts. The first part (up to meter 80) has ratio variations ranging between 0.70762 and 0.70772 whereas, towards the top of the sequence the ratios rise up to 0.70790. The biostratigraphic control allows establishing a Ladinian age (Fassanien) for the lower part of the section (based on the appearance of *Israelites,* and *Gevanites* from the group *G. altecarinatus* at meter 15), and the upper Keuper facies that cap the succession is Carnian in age (Fig. 2). Therefore, when plotting the $^{87}Sr/^{86}Sr$ isotope values with respect to height, it is observed that they correlate with a specific part of the Burke *et al.* (1982) curve, being the values of the lower part of the section similar to those of the Tethys Sea curve (Korte *et al.,* 2003, Fig. 7). From meter 80, at the same level where a sharp reduction of the Sr content is observed and a change detected in the outcrop from marine facies to more continental influenced environments, the $^{87}Sr/^{86}Sr$ ratio appears much higher. When comparing the mineralogy content variations with the $^{87}Sr/^{86}Sr$ values we observe periods with a positive correlation between $^{87}Sr/^{86}Sr$ ratio and rising and a coeval or successive increase of the $CaCO_3$ content that correspond to the main inflexion points of the isotope curve trends. These points are located at three height intervals in the section and they are named surfaces: surface 1 (meter 42.82), surface 2 (meter 59.94) and surface 3 (meter 72).

4. Discussion

In general, this succession corresponds to a Transgressive System Tract followed by an overall upward succession with a progradation pattern characteristic of a Highstand Systems Tract. This sequential arrangement corresponds to a third – order depositional sequence similar to the one described by Aigner and Bachmann (1992) for Muschelkalk facies in Germany and by Pérez-Valera *et al.* (2005) for Triassic Muschelkalk facies from South-East Spain.

4.1. Geochemistry and sequence stratigraphy

The sedimentary evolution of the studied succession permits to interpret the different system tracts, and the elemental analysis complements the facies analysis and helps obtaining a comprehensive knowledge of the geochemical fluctuations that appear to occur in this succession of the upper part of the Middle Triassic in the Iberian Peninsula. The comparison of the $^{87}Sr/^{86}Sr$, Mg/Ca, Sr/Ca ratios, the Mn, Fe, and $CaCO_3$ content vertical variations permit to characterise the environmental conditions where these carbonates were formed and the major surfaces that, in this case, separate 4 different parts.

Strontium isotopic composition of ancient seawater is commonly used as a proxy for understanding the tectonic

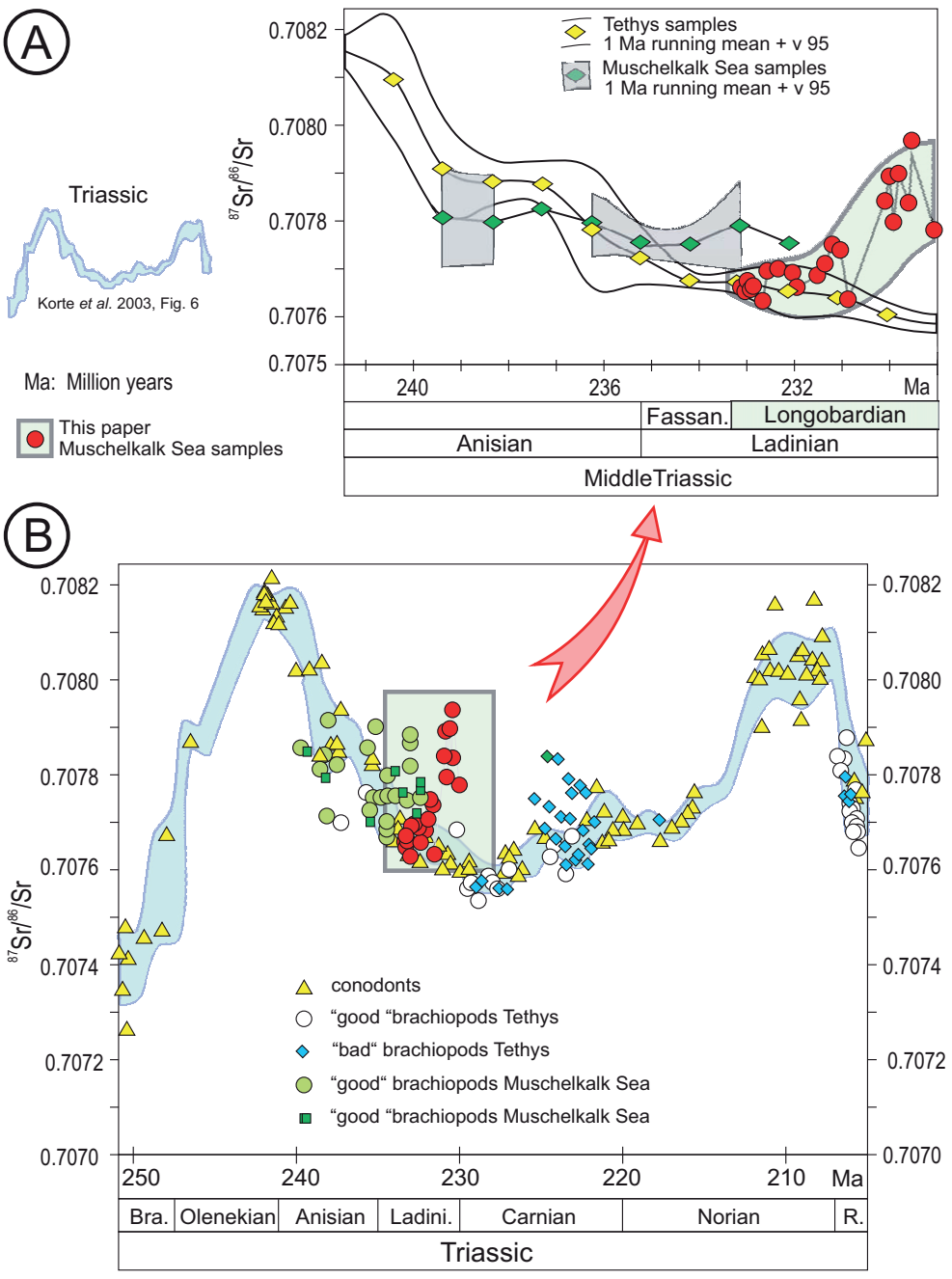

Fig. 7.- Isotopic record of the upper Ladinian westernmost Tethys Sea. A, Comparison of $^{87}Sr/^{86}Sr$ records from this study with the data from Korte *et al.* (2003) for the Tethys and the Muschelkalk seas. The bands width represents the 95 %confidence level of the mean, calculated by student t-test. B, Comparison of the $^{87}Sr/^{86}Sr$ records of this study with data taken from literature (after Korte *et al.* 2003).

evolution of the Earth system as well as a tool for high resolution stratigraphic correlation (Korte *et al.* 2003) and as a climatic indicator (Capo and DePaolo, 1990; Zachos *et al.,* 2001; Veizer *et al.,* 1999; Banner and Hanson, 1990). Sharp changes in the $^{87}Sr/^{86}Sr$ ratio, elements data and mineralogy trends at marked inflexion points (Fig. 6) characterise 3 major surfaces. Surfaces 1 (meter 42.82) appears to mark a rise of the $^{87}Sr/^{86}Sr$ and Sr/Ca ratios, and Mn content, coeval to the lowering of the Mg/Ca ratio and Fe content (Fig. 6). $CaCO_3$ appears to increase values (Fig. 6) for a certain period of time (between meters 42.82 to 48.66). Higher up, surface 2 (meter 59.94) appears characterised by a similar trend in most of the curves (rise of $^{87}Sr/^{86}Sr$ and Sr/Ca ratios and Mn content), and in this case there is a sharp increase of Mn content and Fe. At this surface, the rise of $CaCO_3$ values appears to occur in the following level, and Mg/Ca ratio is stable although it rises as well a bit higher up in the section. Surface 3 (meter 74.49) seems to have similar trend patterns as surface 2 in relation to the $^{87}Sr/^{86}Sr$ ratio, Mn and $CaCO_3$ rapid and sharp rise, whereas Mg/Ca clearly decreases to rise a bit higher up in the section. The higher $^{87}Sr/^{86}Sr$ signatures at surfaces 1, 2 and 3 are indicating major strontium fluxes and their isotope ratios into the ocean water (Burke *et al.,* 1982; Veizer *et al.,* 1999), which could be due to: i) riverine input of radiogenic Sr produced by weathering of continental silicate; ii) Sr derived from hydrothermal circulation produced at mid-ocean ridges (Faure, 1986), likely coincident with second-order sea level fluctuations (Gaffin, 1987). It has been pointed out the existence of a level of high $CaCO_3$ between meters 42.82 to 48.66 that appears co-

incident with a rise of Mn at meter 45.04. The rise of Mn content in surface 1 would support the hydrothermal origin of the Sr input into the ocean, as manganese enrichment of waters and bottom sediments are normally produced by hydrothermal processes at mid-ocean ridges (Edmond *et al.,* 1979). The Mn content in marine carbonates responds as well to variations in sea level and the aragonite to calcite ratio production of the platform (Renard *et al.,* 2005; Jarvis *et al.,* 2001). In response to sea level (Renard *et al,.* 2005) minimum Mn contents appear related to sequence boundaries, a rise is related to transgressive systems and maximum values appear at maximum flooding surfaces, with declining values through the following highstand. In the study area the maximum flooding that defines the point of maximum flooding surface is difficult to identify herein as a single surface and instead it is recognized within a zone (MFZ) where sequential interpretations obtained analysing the Mn curve indicate that surface 1 would represents the maximum flooding surface, and therefore surfaces 2 and 3 (with rises of Mn) would be minor flooding surfaces produced during the Highstand Systems Tract. The Mg/Ca and Sr/Ca ratios are related as well to variations in the hydrothermal activity of the mid-ocean ridges. These ratios are major controlling factors involved in the regulation of the mineralogical nature of inorganic $CaCO_3$ (MacKenzie and Pigott,1981; Wilkinson and Given, 1986). Calcite seas appear following times of rapid seafloor spreading and global greenhouse climate conditions (Stanley and Hardie, 1998). High activity of mid-ocean ridges, produced at the time of maximum flooding surface formation, lead to rapid Ca concentration rise in the sea water that permitted to precipitate carbonate sediments in the restricted subtidal environment (meters 40 to 48). The increase of the dissolved Ca produced a decrease in sea water Sr/Ca ratio. Instead, Mg content lowering in the sea water is slow and progressive due to the long oceanic residence time of the Mg. When the Sr/Ca ratio was stabilized, the Mg/Ca continued to decrease progressively for a longer period as the Mg content decreased. The inverse pattern is observed when hydrothermal activity decreased (from meter 45.04; Fig. 6).

Carbonate contents increase as well in response to rising sea level (Jarvis *et al.,* 2001). Values increase through each Transgressive Systems Tract, reach a maximum around the maximum flooding surface (surface 1) and then remain high and more or less constant through the Highstand Systems Tract (Renard, 1986).

Therefore, a transgressive and deepening trend, supported by the facies association and stacking pattern criteria, appears to be represented in the lower part of the measured section, below the maximum flooding, (surface 1, Fig. 6). The Transgressive Systems Tract (TST) is delineated by a retrogradational growth of offshoal deposits with tempestites on top of intertidal to subtidal deposits, a deep water transgressive wedge. The maximum flooding zone (MFZ) is located between levels 18 and 20 (meters 42.82 to 45.04), where a turnaround from a retrogradational to a progradational stacking trend is produced and inside a geochemical change, surface 1, would represent the maximum flooding surface. This trend is correlated to similar sections in adjacent areas (Pérez-Valera and Pérez-López, 2008; Pérez-López and Pérez-Valera, 2012). The exact location of the maximum flooding zone can be established at the point of $^{87}Sr/^{86}Sr$ rise, together with $CaCO_3$ rise coeval to sea floor spreading, sea level rise and Mn enrichment due to hydrothermal activity. This is coincident with the low Sr/Ca and later stabilization of the Mg/Ca ratios as hydrothermal activity ceased, trends that characterise this type of sequences and observed in the succession (Fig. 6). The shoal deposits change upwards into back shoal and tidal flat prograding deposits, which represent a regressive succession formed in a Highstand System Tract. Surfaces 2 and 3 present similar characters to surface 1, but the facies stacking indicates as well a change in the trend to a progradation. Therefore, these surfaces would represent flooding surfaces produced within a Highstand System Tract. From surface 1 the deposits represent the general progradation of the platform environments towards the sea. Mineralogically and geochemically the flooding surfaces are marked as well by rises of $^{87}Sr/^{86}Sr$ ratios, and abrupt rises in $CaCO_3$ and Mn contents. The juxtaposition of the progradational system and the establishment of transitional, less marine influenced environments on the area is the likely reason for the eventual rise of the $^{87}Sr/^{86}Sr$ ratio at meter 93 (Fig. 6). Normally, it is considered that Sr concentration progressively decreases from open-ocean to offshore, nearshore and to brackish water environments (Cochran *et al.,* 2003). Therefore, this part of the section, characterized by a rapid and net increase in $^{87}Sr/^{86}Sr$ ratio and a general decrease in the Sr content, is interpreted as representing the moment of stabilization on the carbonate production and the emplacement in the area of transitional environments characterized by meteoric and brackish water influenced settings that produced dilution of the seawater with meteoric continental waters (Renard, 1986). This part of the sequence was formed possibly during a period of extremely low humidity that would enhance high erosion and higher material supply form the continent. During the Triassic, the equatorial inner Pangaea was characterized by arid climate conditions, with only monsoonal rains towards the eastern edge of the supercontinent (Crowley, 1994). Progressive erosion of Pangaea highland areas during the Middle Triassic probably stripped off the low-ratio sedimentary cover and exposed older, more radiogenic rocks to weathering that produced material with higher $^{87}Sr/^{86}Sr$ values. The Sr/Ca ratio lowering in the upper part of the sequence, together with the facies analysis and the significant $^{87}Sr/^{86}Sr$ values rise indicate the progradation pattern of the sequence and the establishment of brackish water environment in the area.

Between meters 40 and 80, the $^{87}Sr/^{86}Sr$ data correlates to the values of Korte *et al.* (2003) curve, therefore allowing to attribute this part of the section to an Early Longobardian

age (Fig.7). Higher up in the section (from meter 80) values appear quite different to the cited studies, corroborating the aforementioned interpretation of an environmental change into a brackish water dominated setting in the area. Finally, the fall in sea-level caused the deposition of overlaying Keuper coastal facies.

5. Conclusion

Petrographic and elemental data variations indicate that the samples from the lower part (up to meter 80) of the succession have not undergone significant diagenetic alterations and therefore, the studied carbonate samples contain direct information of their coeval seawater. Moreover, the geochemical analysis of $^{87}Sr/^{86}Sr$ and elements contents and ratios together with the analysis of the architectural arrangements of the facies associations permit to characterise the sequence stratigraphic framework of the studied section. On the contrary, the samples from the upper part of the section (meter 80 to top) show geochemical and mineralogical variations that indicate that the carbonates of this part of the section have been exposed to the influence of diagenetic fluids, and therefore, their values are not of use to be compared to the $^{87}Sr/^{86}Sr$ data curve of Korte *et al.* (2003).

The overall Upper Muschelkalk facies of the "Rambla del Cuchillo" succession is interpreted as representing a gentle slope (ramp-like) epeiric carbonate platform within a transgressive and latter upper regressive third-order relative sea level cycle. The first dolomitic interval overlaying the Buntsandstein facies represents the transgression onset and it has a deepening-upwards trend. The Transgressive Systems Tract (TST) is delineated by a retrogradational growth of offshoal deposits with tempestites, the deep water transgressive wedge and the shoal deposits that change upwards into restricted subtidal and tidal flat progradational deposits, which are a regressive succession formed in a Highstand System Tract. Sea-level fluctuations, marked by geochemical changes, are observed in surfaces 1, 2 and 3. The maximum flooding surface zone (MFZ) is recognized between meters 42 to 45 in the measured section, where a turnaround from a retrogradational to a progradational stacking trend is produced. The geochemical signal of this surface is characterised by a rise in Mn, Fe, $CaCO_3$, Sr/Ca ratio and $^{87}Sr/^{86}Sr$ values, whereas Mg/Ca ratio decreases. The Highstand Systems Tract (HTS), on top of the MFZ, is composed of progradational shoal, backshoal and tidal flat deposits that compose shoaling sequences that indicate the lowering of the sea level in the area. The relative long-lasting subaerial exposure and sharp facies change into an evaporitic salt marsh or salt pan environment of the Keuper facies suggests that a relative sea-level fall and a Lowstand Systems Tract resulted over the upper boundary of the Muschelkalk sequence.

The $^{87}Sr/^{86}Sr$ values of the lower part of the succession are coincident with those of the time equivalent interval of the Tethys curve (Korte *et al.,* 2003), and therefore it serves to establish the detailed Early Longobardian age for this part of the stratigraphic succession. Meanwhile, higher up in the section (from meter 80 and onwards), at the moment of a depositional environment change into continental deposits takes place, the $^{87}Sr/^{86}Sr$ values differ significantly to the Tethys curve. The Sr/Ca ratio lowering in the upper part of the sequence, together with the facies analysis and the significant $^{87}Sr/^{86}Sr$ values rise appear coeval to the progradational pattern of the succession and the establishment of brackish water environments in the area.

Acknowledgements

The authors thank Prof. J. McArthur (Department of Earth Sciences, University College London, England) who provided helpful comments and nice discussions which improved the original manuscript. T A. Pérez-López and an anonymous referee are acknowledged for comments and suggestions that have greatly improved the manuscript. The authors would also like to thank the X Ray Diffraction CAI for XRD and ICP measurements, the Geochronology and Isotopic Geochemistry CAI for $^{87}Sr/^{86}Sr$ ratio values and the Geological Techniques CAI from the University Complutense of Madrid. The research was supported as part of the SEMIARID (CGL2006-01074) Project, funded by the Spanish MEC.

References

Aigner, T., and Bachmann, G. H. (1992): Sequence stratigraphic framework of the German Triassic. *Sedimentary Geology* 80, 115-135. doi:10.1016/0037-0738(92)90035-P.

Aigner, T., and Futterer, E. (1978): Kolk-Töpfe und-Rinnen (pot and gutter casts) im Muschelkalk. Anzeiger für Wattenmeer. *Neues Jahrbuch für Geologie und Paläontologie* 156, 285-304.

Arche, A., López-Gómez, J. (2014): The Carnian Pluvial Event in Western Europe: New data from Iberia and correlation with the Western Neotethys and Eastern North America-NW Africa regions. *Earth-Science Reviews* 128, 196-231. doi:10.1016/j.earscirev.2013.10.012.

Banner, J. L., and Hanson, G. N. (1990): Calculation of simultaneous isotopic and trace-element variations during water-rock interaction with applications to carbonate diagenesis. *Geochimica et Cosmochimica Acta* 54, 3123-3137. doi:10.1016/0016-7037(90)90128-8.

Beltran, C. (2006): Variations des paramètres de l'environnement océanique au cours de la sédimentation d'un doublet marne-calcaire. Approches géochimique, minéralogique et micropaléontologique. Thèse de Doctorat, Université Pierre et Marie Curie. París, *Mémoires des Sciences de la Terre*, 2006-05, 252 p.

Beltran, C., Rafélis, M., De Renard, M., Moullade, M., and Tronchetti, G. (2007): Environmental changes during marl-limestone formation: Evidence from the Gargasian (Middle Aptian) of La Marcouline Quarry (Cassis, SE France). *Brest, Carnets de Géologie/Notebooks on Geology*, article 2007/01, 13 p.

Besems, R. E. (1981a): Aspects of Middle and Late Triassic Palynology. 1. Palynostratigraphical data from the Chiclana de Segura Formation of the Linares-Alcaraz (Southeastern Spain) and correlation with Palynological assemblages from the Iberian Peninsula. *Review of Palaeobotany and Palynology* 32, 257-273. doi:10.1016/0034-6667(81)90007-5.

Besems, R. E. (1981b): Aspects of Middle and Late Triassic Palynology.

2. Preliminary Palynological data from the Hornos-Siles Formation of the Prebetic zone, NE province of Jaen (Southeastern Spain). *Review of Palaeobotany and Palynology* 32, 389-400. doi:10.1016/0034-6667(81)90020-8.

Bourquin, S., Bercovici, A., López-Gómez, J., Díez, J. B., Broutin, J., Ronchi, A., Durand, M., Arche, A., Linol, B., and Amour, F. (2011): The Permian-Triassic transition and the onset of Mesozoic sedimentation at the northwestern peri-Tethyan domain scale: Palaeogeographic maps and geodynamic implications. *Palaeogeography Palaeoclimatology Palaeoecology* 299, 265-280. doi:10.1016/j.palaeo.2010.11.007.

Brack, P., Rieber, H., and Nicora, A. (2003): The Global Stratigraphic Section and Point (GSSP) of the base of Ladinian Stage (Middle Triassic). *Albertiana* 28, 13-25.

Brack, P., Rieber, H., Nicora, A., and Mundil, R. (2005): The Global boundary Stratotype Section and Point (GSSP) of the Ladinian Stage (Middle Triassic) at Bagolino (Southern Alps, Northern Italy) and its implications for the Triassic time scale. *Episodes* 28, 233-244.

Brand, U., and Veizer, J. (1980): Chemical diagenesis of a multicomponent carbonate system-1: trace elements. *Journal of Sedimententary Petrology* 50, 1219-1236. doi:10.1306/212F7BB7-2B24-11D7-8648000102C1865D.

Bruckschen, P., Oesmann, S., and Veizer, J. (1999): Isotope stratigraphy of the European Carboniferous: proxy signals for ocean chemistry, climate and tectonics. *Chemical Geology* 161,127-163. doi:10.1016/S0009-2541(99)00084-4.

Burke, W. H., Denison, R. E., Hetherington, E. A., Koepnick, R. B., Nelson, H. F., and Otto, J. B. (1982): Variation of seawater $^{87}Sr/^{86}Sr$ throughout Phanerozoic time. *Geology* 10, 516-519. doi: 10.1130/0091-7613(1982)10<516:VOSSTP>2.0.CO;2.

Calvet, F., Tucker, M. E., and Henton, M. (1990): Middle Triassic carbonate ramp systems in the Catalan Basin, northeast Spain: facies, systems tracts, sequences and controls. *Special Publications of International Association of Sedimentologists* 9, 79-108.

Capo, R. C., and DePaolo, D. J. (1990): Seawater Strontium Isotopic Variations from 2.5 Million Years Ago to the Present. *Science* 249, 51-55. doi: 10.1126/science.249.4964.51.

Chambers, J. M., Cleveland, W. S., Kleiner, B., and Tukey, P. A. (1983): *Graphical methods for data analysis*. Belmont, Wadsworth, 395 p.

Cleveland, W. S. (1979): Robust locally weighted regression and smoothing scatterplots. *Journal of American Statistical Association* 74, 829-836. doi: 10.1080/01621459.1979.10481038.

Cleveland, W. S., Grosse, E., and Shyu, W. M. (1992): Local regression models. In: Chambers J. M., Hastie, T., (eds.), *Statistical Models*. New York, Chapman and Hall, pp. 309-376.

Cochran, J. K., Kallenberg, K., Landman, N. H., Harries, P. J., Weinreb, D., Turekian, K. K., Beck, A. J., and Cobban, W. A. (2010): Effect of diagenesis on the Sr, O, and C isotope composition of late Cretaceous mollusks from the Western Interior Seaway of North America. *American Journal of Science* 310, 69-88. doi: 10.2475/02.2010.01.

Cochran, J. K., Landman, N. H., Turekian, K. K., Michard, A., and Schrag, D. P. (2003): Paleoceanography of the Late Cretaceous (Maastrichtian). Western Interior Seaway of North America: Evidence from Sr and O isotopes. *Palaeogeography Palaeoclimatology Palaeoecolology* 191, 45-64. doi:10.1016/S0031-0182(02)00642-9.

Crowley, T. J. (1994): Pangean climates. *Geological Society of America Special Papers* 288, 25-40. doi: 10.1130/SPE288-p25.

Cohen, A.L., Owens, K.E., Layne, G.D., and Shimizu, N. (2002): The effect of algal symbionts on the accuracy of Sr/Ca paleotemperatures from coral. *Science* 296, 331-333. doi: 10.1126/science.1069330.

De Torres, T. (1990): Primeros resultados de unas dataciones palinológicas en el Keuper de la Rama Castellana de la Cordillera Ibérica, Prebético y Subbético frontal. In: Ortí, F., Salvany, J. M. (eds), *Formaciones evaporíticas de la Cuenca del Ebro y cadenas periféricas y de la zona de Levante.* Enresa, Barcelona, pp. 229-223.

De Vicente, G., Vegas, R., Muñoz-Martín, A., Van Wees, J. D., Casas-Sáinz, A., Sopeña, A., Sánchez-Moya, Y., Arche, A., López-Gómez, J., Oláiz, A., and Fernández-Lozano, J. (2009): Oblique strain partitioning and transpression on an inverted rift: The Castilian Branch of the Iberian Chain. *Tectonophysics* 470, 224-242. doi:10.1016/j.tecto.2008.11.003.

Dunham, R. J. (1962): Classification of carbonate rocks according to depositional texture. In: Ham, W. E (ed). *Classification of carbonate rocks*. American Association of Petroleum Geologists Memoir 1, 108-121.

Edmond, J. M., Measures, C., McDuff, R. E., Chan, L. H., Collier, R., and Grant, B. (1979): Ridge crest hydrothermal activity and the balances of the major and minor elements in the ocean; the Galapagos data. *Earth and Planetary Science Letters* 46, 1-18. doi:10.1016/0012-821X(79)90061-X.

Escavy, J.I., Herrero, M.J., Arribas, M.E. (2012): Gypsum resources of Spain: Temporal and spatial distribution, *Ore Geology Reviews* 49, 72-84. doi:10.1016/j.oregeorev.2012.09.001 .

Escudero-Mozo, M. J., Márquez-Aliaga, A., Goy, A., Martín-Chivelet, J., López-Gómez, J., Márquez, L., Arche, A., Plasencia, P., Pla, C., Marzo, M., and Sánchez-Fernández, D. (2015): Middle Triassic carbonate platforms in easter Iberia: Evolution of their fauna and palaeogeographic significance in the western Tethys. *Palaeogeography Palaeoclimatology Palaeoecolology* 417, 236-260. doi:10.1016/j.palaeo.2014.10.041.

Faure, G. (1986): The Rb-Sr method of dating. In: *Principles of Isotope Geology*. John Wiley and Sons, New York,. pp. 117-140.

Fernández, J., and Pérez-López, A. (2004): Triásico. In: Vera, J. A. (ed.), *Geología de España*. Sociedad Geológica de España-Instituto Geológico y Minero de España, Madrid, pp. 365-366.

Gaffin, S. (1987): Ridge volume dependence on sea-floor generation rate and inversion using long-term sea level change. *American Journal of Science* 287, 596-611. doi: 10.2475/ajs.287.6.596.

Goy, A. (1995): Ammonoideos del Triásico Medio de España: Bioestratigrafía y Correlaciones. *Cuadernos de Geología Ibérica* 19, 21-60.

Jacobsen, S. B., and Kaufman, A. J. (1999): The Sr, C and O isotopic evolution of Neoproterozoic seawater. *Chemical Geology* 161, 37-57. doi:10.1016/S0009-2541(99)00080-7.

Jarvis, I., Murphy, A. M., and Gale, A. S. (2001): Geochemistry of pelagic and hemipelagic carbonates: criteria for identifying systems tracts and sea-level change. *Journal of the Geological Society, London* 158, 685-696. doi: 10.1144/jgs.158.4.685.

Korte, C., Kozur, H. W., Bruckschen, P., and Veizer, J. (2003): Strontium isotope evolution of Late Permian and Triassic seawater. *Geochimica et Cosmochimica Acta* 67, 47-62. doi:10.1016/S0016-7037(02)01035-9.

López-Gómez, J., Arche, A., and Pérez-López, A. (2002): Permian and Triassic. In: Gibbons, W., Moreno, T. (eds.), *The Geology of Spain*. Geological Society, London, pp. 185-212.

Lowenstein, T.K., Timofeeff, M.N., Brennan, S.T., Hardie, L.A., and Demicco, R.V. (2001): Oscillations in Phanerozoic Seawater Chemistry: Evidence from Fluid Inclusions. *Science* 294, 1086-1088. doi: 10.1126/science.1064280.

Mackenzie, F. T., and Pigott, J. D. (1981): Tectonic controls of Phanerozoic sedimentary rock cycling. *Journal of the Geological Society London* 138, 183-196.doi: 10.1144/gsjgs.138.2.0183.

Márquez-Aliaga, A., and Ros, S. (2003): Associations of bivalves of Iberian Peninsula (Spain): Ladinian. *Albertiana* 28, 85-89.

Marshall, J. D. (1992): Climatic and oceanographic isotopic signals from the carbonate rock record and their preservation. *Geological Magazine* 129, 143-160. doi:10.1017/S0016756800008244.

McArthur, J. M., Howarth, R. J., and Bailey, T. R. (2001): Strontium Isotope Stratigraphy: Lowess Version 3: Best Fit to the Marine Sr-

Isotope Curve for 0-509 Ma and Accompanying Look-up Table for Deriving Numerical Age. *Journal of Geology* 109, 155-170. doi: 10.1086/319243.

McArthur, J. M., Thirlwall, M. F., Engkildec, M., Zinsmeister, W. J., and Howartha, R. J. (1998): Strontium isotope profiles across K/T boundary sequences in Denmark and Antarctica. *Earth and Planetary Science Letters* 160, 179-192. doi:10.1016/S0012-821X(98)00058-2.

Mercedes-Martín, R., Salas, R., and Arenas, C. (2014): Microbial-dominated carbonate platforms during the Ladinian rifting: sequence stratigraphyand evolution of accommodation in a fault-controlled setting (Catalan Coastal Ranges,NESpain). *Basin Research* 26, 269-296. doi:10.1111/bre.12026.

Myrow, P. M. (1992a): Bypass-zone tempestite facies model and proximality trends for an ancient muddy shoreline and shelf. *Journal of Sedimententary Petrology* 62, 99-115. doi: 10.1306/D426789D-2B26-11D7-8648000102C1865D.

Myrow, P. M. (1992b): Pot and gutter casts from the Chapel Island Formation, southeast Newfoundland. *Journal of Sedimententary Petrology* 62, 992-1007. doi: 10.2110/jsr.62.992.

Nieto, L. M., Ruiz-Ortiz, P. A., Rey, J., and Benito, M. I. (2008): Strontium-isotope stratigraphy as a constraint on the age of condensed levels: examples from the jurassic of the subbetic Zone (southern Spain). *Sedimentology* 55, 1-29. doi: 10.1111/j.1365-3091.2007.00891.x.

Pérez-López, A. (1996): Sequence model for coastal-plain depositional systems of the Upper Triassic (Betic Cordillera, southern Spain). *Sedimentary Geology* 101, 99-117. doi:10.1016/0037-0738(95)00050-X.

Pérez-López, A. (2001): Significance of pot and gutter cast in the Middle Triassic carbonate platform, Betic Cordillera, southern Spain. *Sedimentology* 48, 1371-1388. doi: 10.1046/j.1365-3091.2001.00425.x.

Pérez-López, A., and Pérez-Valera, F. (2012): Tempestite facies models for epicontinental Triassic carbonates of the Betic Cordillera. (Southern Spain). *Sedimentology* 59, 646-678. doi: 10.1111/j.1365-3091.2011.01270.x.

Pérez-López A., and Pérez-Valera F., and Götz A.E. (2012): Record of epicontinental platform evolution and volcanic activity during a major rifting phase: The Late Triassic Zamoranos Formation (Betic Cordillera, S Spain). *Sedimentary Geology* 247-248, 39-57. doi:10.1016/j.sedgeo.2011.12.012.

Pérez-López, A., Solé de Porta, N., Márquez Sanz, L., and Márquez-Aliaga, A. (1992): Caracterización y datación de una unidad carbonática de edad Noriense (Fm. Zamoranos) en el Trías de la Zona Subbética. *Revista de la Sociedad Geológica de España* 5, 113-127.

Pérez-Valera, F., and Pérez-López, A. (2008): Stratigraphy and sedimentology of Muschelkalk carbonates of the Southern Iberian Continental Palaeomargin (Siles and Cehegín Formations, Southern Spain). *Facies* 54, 61-87. doi: 10.1007/s10347-007-0125-1.

Pérez-Valera, J. A., Pérez-Valera, F., and Goy, A. (2005): Bioestratigrafía del Ladiniense Inferior en la región de Calasparra (Murcia, España). *Geo-Temas* 8, 211-215.

Pratt, B. R., and James, N. P. (1986): The St. George Group (lower Ordovician) of western Newfoundland: tidal flat island model for carbonate sedimentation in epeiric seas. *Sedimentology* 33, 313-343. doi: 10.1111/j.1365-3091.1986.tb00540.x.

Ramos, A., Sopeña, A., and Pérez-Arlucea, M. (1986): Evolution of Buntsandstein Fluvial Sedimentation in the Northwest Iberian Ranges (Central Spain). *Journal of Sedimentary Petrology* 56, 862-875. doi:10.1306/212F8A6C-2B24-11D7-8648000102C1865D.

Rausch, S., Böhm, F., Bach, W., Klügel, A., and Eisenhauer, A. (2013): Calcium carbonate veins in ocean crust record a threefold increase of seawater Mg/Ca in the past 30 million years. *Earth and Planetary Science Letters* 362, 215-224. doi:10.1016/j.epsl.2012.12.005.

Renard, M. (1985): *Géochimie des carbonates pélagiques: Mise en évidence des fluctuations de la composition des eaux océaniques depuis 140 MA*. Documents du BRGM 85, Orléans, 650 p.

Renard, M. (1986): Pelagic carbonate chemostratigraphy (Sr, Mg, ^{18}O, ^{13}C). *Marine Micropaleontology* 10, 117-164. doi:10.1016/0377-8398(86)90027-7.

Renard, M., Rafélis, M., Emmanuel, L., Moullade, M., Masse, J. P., Kuhnt, W., Bergen, J. A., and Ronchetti, G. (2005): Early Aptian δ13C and manganese anomalies from the historical Cassis-La Bédoule stratotype sections (S.E. France): relationship with a methane hydrate dissociation event and stratigraphic implications. Brest, *Carnets de Géologie/ Notebooks on Geology.* Available http://paleopolis.rediris.es/cg/CG2005_A04/.

Rodríguez-Tovar, F. J., and Pérez-Valera, F. (2008): Trace Fossil Rhizocorallium From The Middle Triassic Of The Betic Cordillera, Southern Spain: Characterization And Environmental Implications. *Palaios* 23, 78-86. doi: 10.2110/palo.2007.p07-007r.

Rosales, I., Quesada, S., and Robles, S. (2001): Primary and diagenetic isotopic signals in fossils and hemipelagic carbonates: the Lower Jurassic of northern Spain. *Sedimentology* 48, 1149-1169. doi: 10.1046/j.1365-3091.2001.00412.x.

Solé de Porta, N., and Ortí, F. (1982): Primeros datos crontoestratigráficos de las series evaporíticas del triásico superior de Valencia (España). *Acta Geologica Hispanica* 17, 185-191.

Sopeña, A. (2004): Cordillera Ibérica y Costero Catalana. In: Vera, J.A., (ed.) *Geología de España*. Sociedad Geológica de España-Instituto Geológico y Minero de España, Madrid. pp 465-527.

Sopeña, A., Doubinger, J., Ramos, A., and Pérez-Arlucea, M. (1995): Palynologie du Permien et du Trias dans le Centre de Péninsule Ibérique. *Sciences Géologiques Bulletin* 48, 119-157.

Sopeña, A., López, J., Arche, A., Pérez-Arlucea, M., Ramos, A., Virgili, C., and Hernando, S. (1988): Permian and Triassic rift basins of the Iberian Peninsula. In: Manspeizer, W. (ed.), *Triassic-Jurassic rifting.* Developments in Geotectonics. Elsevier, Amsterdam, 22B, pp. 757-786.

Sopeña, A., Ramos, A., and Villar, M. V. (1990): El Triásico del sector Alpera-Montealegre del Castillo (Prov. de Albacete). In: Ortí, F., Salvany, J.M. (eds.), *Formaciones evaporíticas de la Cuenca del Ebro y cadenas periféricas, y de la zona de Levante*. Enresa, Barcelona, pp. 224-231.

Sopeña, A., Sánchez-Moya, Y., and Barrón, E. (2009): New palynological and isotopic data for the Triassic of the Western Cantabrian Mountains (Spain). *Journal of Iberian Geology* 35, 35-45.

Stampfli, G. M., and Borel, G. D. (2002): A plate tectonic model for the Palaeozoic and Mesozoic constrained by dynamic plate boundaries and restored synthetic oceanic isochrones. *Earth and Planetary Science Letters* 196, 17-33. doi:10.1016/S0012-821X(01)00588-X.

Stanley, S. M., and Hardie, L. A. (1998): Secular oscillations in the carbonate mineralogy of reef-building and sediment-producing organisms driven by tectonically forced shifts in seawater chemistry. *Palaeogeography Palaeoclimatology Palaeoecolology* 144, 3-19. doi:10.1016/S0031-0182(98)00109-6.

Thisted, R. A. (1988): *Elements of Statistical Computing: Numerical Computation*. Chapman and Hall, New York, 427 p.

Van der Eem, J. (1983): Aspects of Middle and Late Triassic palinology. 6. Palinological investigations in the Ladinian and Lower Karnian of Western Dolomites, Italy. *Review of Palaeobotany and Palynology* 39, 189-300. doi:10.1016/0034-6667(83)90016-7.

Veizer, J. (1983): Trace elements and isotopes in sedimentary carbonates. *Reviews in Mineralogy and Geochemistry* 11, 265-300.

Veizer, J. (1995): Reply to the comment by L.S. Land on 'Oxygen and carbon isotopic composition of Ordovician brachiopods: implications for coeval seawater. *Geochimica et Cosmochimica Acta* 59, 2845-2846. doi:10.1016/0016-7037(95)00177-2.

Veizer, J., Ala, D., Azmy, K., Bruckschen, P., Buhl, D., Bruhn, F., Carden, G. A. F., Diener, A., Ebneth, S., Godderis, Y., Jasper, T., Korte, C., Pawellek, F., Podlaha, O.G., and Strauss, H. (1999): $^{87}Sr/^{86}Sr$, d13C

and d18O evolution of Phanerozoic seawater. *Chemical Geology* 161, 59-88. doi:10.1016/S0009-2541(99)00081-9.

Wenzel, B., L´ecuyer, C., and Joachimski, M. M. (2000): Comparing oxygen isotope records of Silurian calcite and phosphate-d^{18}O compositions of brachiopods and conodonts. *Geochimica et Cosmochimica Acta* 64, 1859-1872. doi:10.1016/S0016-7037(00)00337-9.

Wilkinson, B. H., and Given, K. R. (1986): Secular variation in abiotic marine carbonates: constraints on Phanerozoic atmospheric carbon dioxide contents and oceanic Mg/Ca ratios. *Journal of Geology* 94, 321-333. doi: 10.1086/629032.

Zachos, J., Pagani, M., Sloan, L., Thomas, E., and Billups, K. (2001): Trends, rhythms and aberrations in global climate 65Ma to present. *Science* 292, 686-693. doi: 10.1126/science.1059412.

Ziegler, P. A. (1990): *Geological Atlas of Western and Central Europe* (2nd edition). Shell International Petroleum Mij BV, The Hague, 232 p.

Ziegler. P. A., and Stampfli, G. M. (2001): Late Palaeozoic-Early Mesozoic plate boundary reorganization: collapse of the Variscan Orogen and opening of Neotethys. Brescia: *Annali di Museo Civico di Storia Naturale*, Monografía 25, 17-34.